35th International Electric Vehicle Symposium and Exhibition (EVS35)
Oslo, Norway, June 11-15, 2022

Vertical vibration reduction by new electric motor control in dry sand condition

Akira Sawada, Jun Motosugi, Nagatoshi Seki, Kengo Fujiwara, Takashi Nakajima

Nissan Motor Co., Ltd. 560-2 Okatsukoku, Atsugi-shi, Kanagawa 243-0192, Japan,

a-sawada@mail.nissan.co.jp

Summary

This paper describes a study on the vertical vibration of electric vehicles in dry sand conditions. This phenomenon can be explained by considering the traction wheel slip and was simulated using the vehicle vibration model. This approach can also explain the difference in vibration behavior between conventional powertrain vehicles and electric vehicles. In addition, a new electric motor control system to reduce the vertical vibration is proposed.

Keywords: EV (electric vehicle), electric drive, off-road, traction control, simulation

1 Introduction

In recent years, the development of vehicles powered by electric motors has accelerated in response to social demands for environmental protection. Examples include electric vehicles (EVs) and hybrid EVs. EVs powered by electric motors are markedly superior to conventional vehicles that use gasoline and diesel engines in terms of torque response. However, a steep torque input into an EV can produce torsional vibration (felt as a shaking vibration) in the powertrain system, causing a significant decline in riding comfort. To strike a balance between vehicle acceleration performance and ride comfort, a shaking vibration control system is proposed, which applies a perfect zeroing method [1] to cancel a specific frequency disturbance without a phase delay.

Evaluations of EVs under various driving conditions have increased, and vertical vibrations in dry sand or deep snow conditions, which reduce ride comfort, are a focus of research and development. Although a driving force control system that considers the characteristics of tire sinkage on sandy roads has been proposed [2] [3], it is also necessary to consider the nonlinear tire slip and suspension characteristics of vibration during vertical acceleration. Thus, a vertical vibration model of a dry sand condition is constructed [4], which considers the road surface reaction force acting on the tire, tire sinkage, and running resistance in dry sand conditions. The validity of this model and the vertical acceleration mechanism were confirmed experimentally for sand and deep snow roads. In this study, a new motor control system is proposed. It is designed based on a physical model, which suppresses the vertical acceleration in dry sand conditions.

2 Vertical Vibration in dry sand conditions

First, the vertical acceleration of the vehicle body in dry sand conditions is described using experimental data from a front-wheel-drive EV. The vehicle parameters are listed in Table 1. The dry sand conditions represent our test course. With regard to vertical acceleration, the responses of the vehicle body and tires were measured with a sensor, as shown in Figure 1.

Table 1: Vehicle Parameter

	Electric vehicle	Conventional vehicle
Vehicle Type	C-SUV	←
Power train	Electric Motor Driven	Engine Driven
Tire width[m]	0.225	←
Tire Radius[m]	0.338	←
Weight[kg]	1860	1520

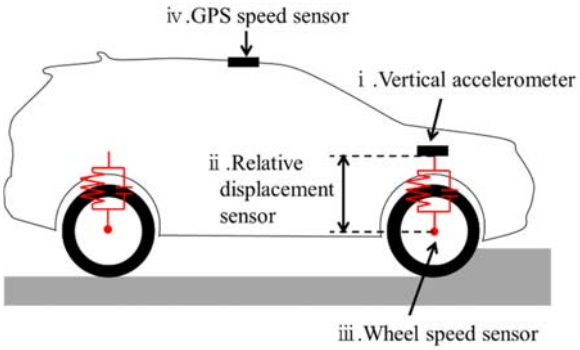

Figure 1: Measurement points

The measured vertical acceleration data are plotted in Figure 2. Figure 2-a shows the electric-motor-driven vehicle results, and the continuous fluctuations of the vertical acceleration of the vehicle body and the traction wheel speed. Figure 2-b shows the conventional powertrain vehicle results and the transient fluctuations of the vertical acceleration of the vehicle body and the traction wheel speed.

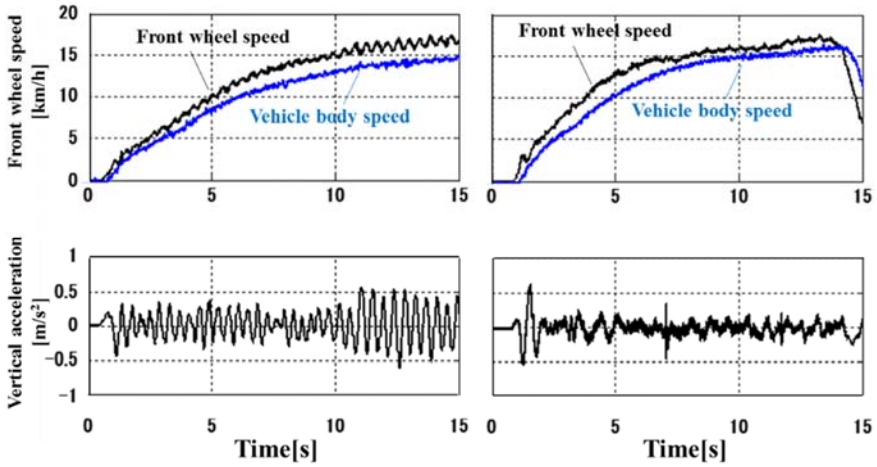

Figure 2-a: electric-motor-driven vehicle Figure 2-b: conventional powertrain vehicle.

Figure 2: The measured vertical acceleration data

3 Vertical vibration simulation

3.1 Vertical vibration model

In considering the mechanism of the vertical acceleration, we attempted to construct a driving force transmission system model for an electric-motor-driven vehicle. The vertical vibration model in dry sand conditions is shown in Figure 3. A longitudinal vehicle model is applied to electric-motor-driven vehicles. The vehicle velocity V and angular velocity of the drive wheel ω_w are calculated from the motor torque T_e, sand resistance F_d, and vertical force F_z. The sand sinkage z_t is calculated from the vertical force F_z and the slip characteristic between the vehicle velocity V and the angular velocity of the drive wheel ω_w. The sand resistance F_d is calculated from the sand sinkage z_t. The vertical vehicle model considers the vehicle mass, tire mass, and suspension system characteristics. The vertical force F_z and suspension displacement z_{m2} are calculated from the sand sinkage z_t.

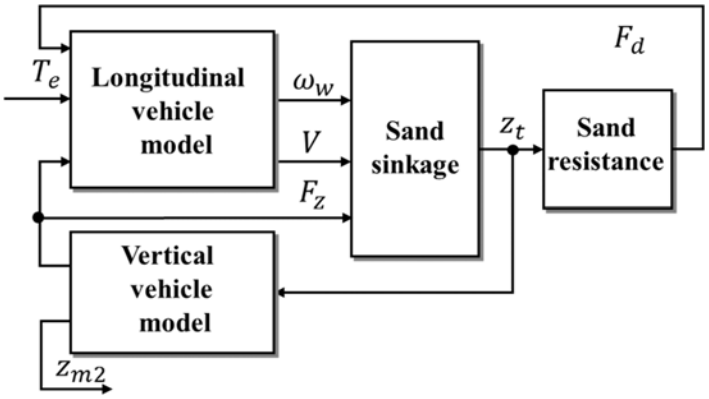

Figure 3: Vertical vibration model

3.2 Vertical motion

It is important to obtain the running resistance for the construction of the vertical vibration model, and it is necessary to derive the running resistance on sand. The sand resistance parameters are shown in Figure 4. When the driving force is generated while the tire sinks and pushes the sand away, it acts in the tangential direction of the contact surface between the tire and sand. The sand resistance F_d is in the horizontal direction of the surface pressure p generated by the wheel load and is expressed by equation (1). The sand resistance F_d is a function of the contact surface angle θ between the tire and sand.

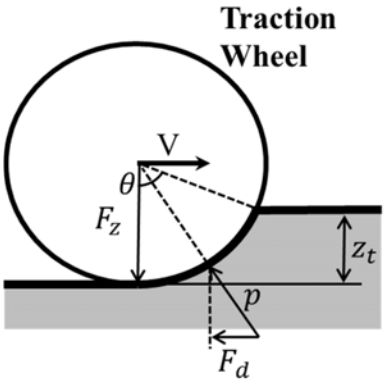

Figure 4: Sand resistance parameters

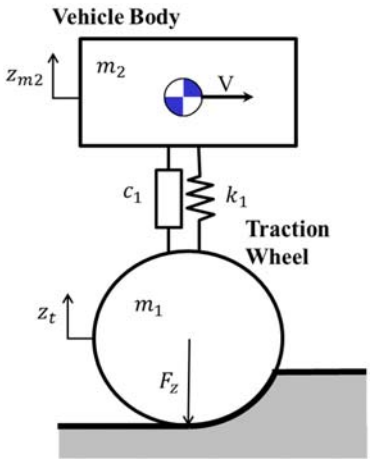

Figure 5: Forward and back movement model of vehicle

$$F_d = \mu F_z + rb \int p(\theta) sin\,\theta d\theta \quad (1)$$

When the contact surface angle θ between the tire and sand is approximated by the proportional equation of the tire sinkage z_t, the sand resistance F_d is expressed as equation (2).

$$F_d = \mu F_z + rb f_0 z_t \quad (2)$$

b	:	tire width	g	:	gravitational acceleration
p	:	tire contact pressure	F_z	:	wheel load
μ	:	road friction coefficient	F_d	:	driving resistance
r	:	radius of tire load	θ	:	contact surface angle between tire
f_0	:	sand resistance factor			and sand

The tire sinkage z_t is represented as the sum of the transient sinkage z_d and steady sinkage z_0. Equation (4) was obtained from reference [2]. The transient sinkage z_d is assumed to be proportional to the tire slip amount and is expressed as equation (3). The steady sinkage z_0 is determined by tire sinkage according to tire load and is expressed as equation (4). The tire sinkage z_t is represented as the sum of the transient sinkage z_d and steady sinkage z_0, which are filtered by the first-order delay according to the vehicle body velocity. Thus, the tire sinkage z_t is expressed as equation (5).

$$z_d = c_0(r\omega_w - V) \quad (3)$$

$$z_0 = a_0 F_z + a_1 \quad (4)$$

$$z_t = \frac{1}{\tau_z s+1}(z_d + z_0) \quad (5)$$

$$\tau_z = \frac{1}{e_0 V}$$

c_0	:	slip sinkage parameter	a_0	:	static sinkage parameter1
V	:	vehicle velocity	a_1	:	static sinkage parameter2
ω_w	:	angular velocity of drive wheel	e_0	:	transient response parameter
s	:	Laplace operator			

The wheel load in the vertical direction of the tire is shown in Figure 5. The suspension displacement z_{m2} is assumed to be the same as the tire sinkage z_t and is expressed as equation (6). The wheel load in the vertical direction of tire F_z is expressed as equation (7).

$$z_{m2} = \frac{c_1 s+k_1}{m_2 s^2+c_1 s+k_1} z_t \quad (6)$$

$$F_z = (m_1 + m_2)g + c_1 \frac{d}{dt}(z_{m2} - z_t) + k_1(z_{m2} - z_t) \quad (7)$$

m_1	:	unsprung mass	k_1	:	spring constant
m_2	:	sprung mass	c_1	:	spring damping coefficient
z_{m2}	:	vertical displacement of body			

3.3 Longitudinal motion

Figure 6 and Figure 7, respectively, show the models of the drive torque transmission system of an EV and the forward/backward motion of the vehicle body. The equations of motion for the vehicle represented in Figure 6 and Figure 7 are expressed as shown below in Equation (8).

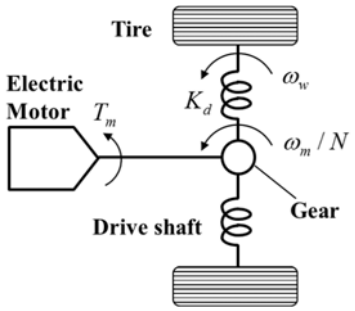

Figure 6: Driving torque transmission model

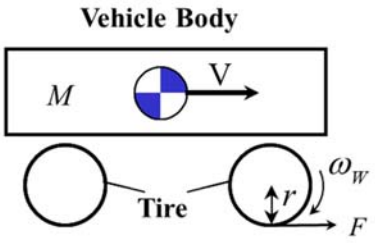

Figure 7: Forward and back movement model of vehicle

$$
\begin{aligned}
J_m \frac{d}{dt}\omega_m &= T_m - \frac{T_d}{N} \\
2J_w \frac{d}{dt}\omega_w &= T_d - rF \\
M\frac{d}{dt}V &= F - F_d \\
T_d &= K_d \int \left(\frac{\omega_m}{N} - \omega_w\right) dt \\
F &= K_t(r\omega_w - V)
\end{aligned}
\tag{8}
$$

J_m	:	motor inertia	T_m	:	motor torque
J_w	:	drive wheel inertia (for one wheel)	T_d	:	drive shaft torque
M	:	equivalent vehicle mass	F	:	driving force
K_d	:	torsional stiffness of drive shaft	N	:	overall gear ratio

The driving force F is calculated according to the slip amount of the tire ($r\omega_w - V$) as shown in Figure 8, and is divided into linear and non-linear regions. In the linear region, the driving force increases according to the amount of slip. In non-linear region, the driving force is limited regardless of the amount of slip. Maximum driving force F_{max} in the non-linear region is calculated according to wheel load F_z.

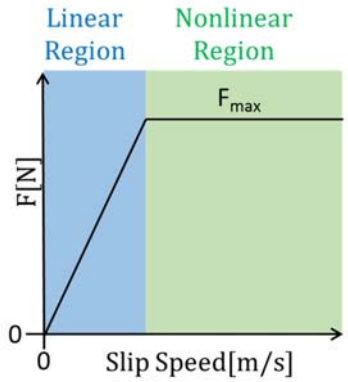

Figure 8: Traction characteristic on sands

Although the transfer function from the slip speed to traction F in the nonlinear region becomes a high-order filter, it can be approximated by equation (9).

$$F = \frac{1}{\tau_{kt}s+1} \cdot K_{slip}(r\omega_w - V) \tag{9}$$

K_{slip} : coefficient of friction between tires and road surface

τ_{kt} : overall vertical transient characteristics

Based on the equations (8) and (9), the transfer function $G_p(s)$ consisting of the input and the motor angular velocity as the output are found with the following equations (10) and (11).

$$\omega_m = G_p(s)\, T_m \tag{10}$$

$$G_p(s) = \frac{1}{s} \cdot \frac{\beta_4 s^4 + \beta_3 s^3 + \beta_2 s^2 + \beta_1 s + \beta_0}{\alpha_4 s^4 + \alpha_3 s^3 + \alpha_2 s^2 + \alpha_1 s + \alpha_0} \tag{11}$$

The constants are defined as follows:

$$\alpha_4 = 2J_m J_w M\tau_{kt} \qquad \beta_4 = 2J_w M\tau_{kt}$$
$$\alpha_3 = 2J_m J_w M \qquad \beta_3 = 2J_w M$$
$$\alpha_2 = K_t J_m(2J_w + r^2 M) \qquad \beta_2 = K_t(2J_w + r^2 M) + K_d M\tau_{kt}$$
$$\alpha_1 = K_d M(J_m + 2J_w/N^2) \qquad \beta_1 = K_d M$$
$$\alpha_0 = K_d K_t(J_m + 2J_w/N^2 + r^2 M/N^2) \qquad \beta_0 = K_d K_t$$

Next, equation (11) is reorganized to obtain equation (12) expressed as:

$$G_p(s) = \frac{M_p}{s} \cdot \frac{(s^2+2\zeta_{z1}\omega_{z1}s+{\omega_{z1}}^2)\cdot(s^2+2\zeta_{z2}\omega_{z2}s+{\omega_{z2}}^2)}{(s^2+2\zeta_{p1}\omega_{p1}s+{\omega_{p1}}^2)\cdot(s^2+2\zeta_{p2}\omega_{p2}s+{\omega_{p2}}^2)} \tag{12}$$

The frequency characteristics of the motor angular velocity were determined in relation to the motor torque. The simulation results are shown in Figure 9. In the linear region, the results indicate that the vehicle has a pronounced resonance characteristic at approximately 10 Hz (ω_{p2}), which is related to the drive shaft torsional vibration. In the nonlinear region, the vehicle has a pronounced resonance characteristic at approximately 3 Hz (ω_{p1}), which is not related to the drive shaft torsional vibration.

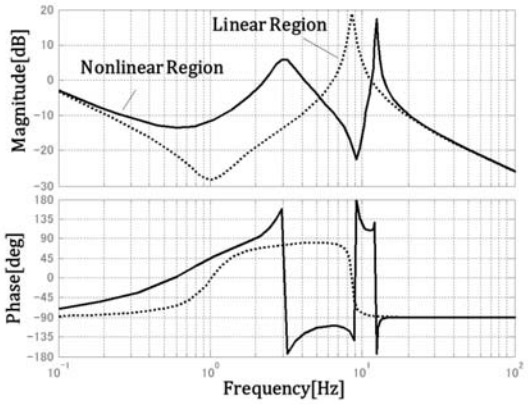

Figure 9: Frequency response of EV on sands.

The difference in behaviour between the conventional powertrain vehicle and the electric-motor-driven vehicle was indicated by simulation in Chapter 2. Here, this behaviour is analysed with the vertical vibration model. The simulation results of the electric-motor-driven vehicle and the conventional powertrain vehicle are shown in Figure 10. The dashed and solid lines represent the results of the conventional powertrain vehicle and electric-motor-driven vehicle, respectively. Conventional powertrain vehicles have less vertical vibrations. Because the conventional powertrain has a larger engine inertia and transmission than the electric-motor-driven powertrain, motor speed fluctuations and vertical vibrations are reduced. We considered it feasible to reduce vertical vibration by suppressing changes in the tire rotational speed due to road surface disturbance by controlling the EV motor.

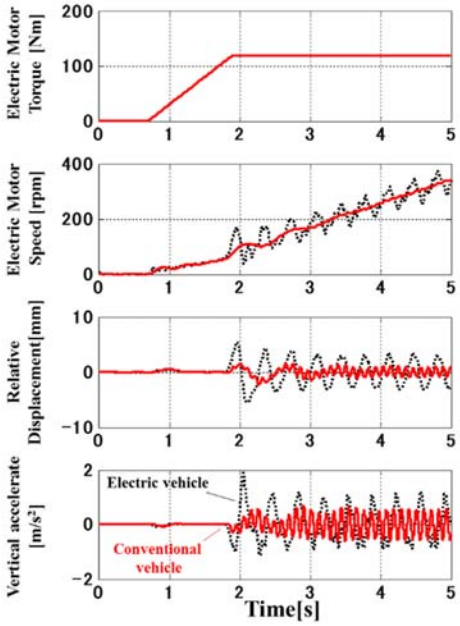

Figure 10: Simulation results of electric-motor-driven vehicle and conventional powertrain vehicle.

4 Electric motor control system

We applied a new electric motor control strategy that reduces the motor speed fluctuations and vertical vibrations in dry sand conditions because of tire rotational speed due to road surface disturbance. Figure 11 shows the configuration of the electric motor control system. The vehicle control module determines the motor torque command values according to the vehicle state, including the accelerator pedal angle, vehicle speed, and state of charge of the lithium-ion battery. The motor controller controls the motor torque T_e via the power device according to the motor torque command values received from the vehicle control module. The drive shaft torsional vibration control system was incorporated into the motor controller.

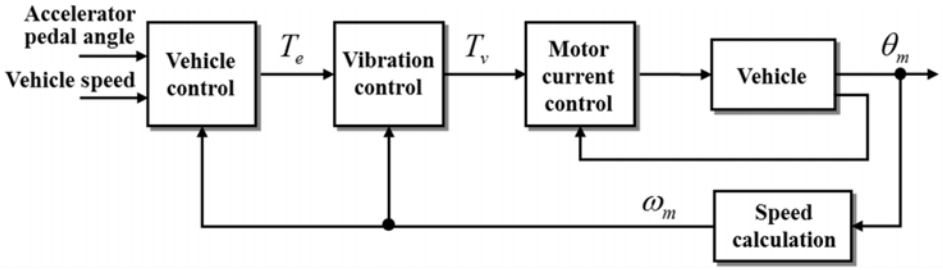

Figure 11: Configuration of electric motor control system

4.1 The proposed vibration control system

Figure 12 shows the configuration of the new electric motor control system that can suppress the vertical acceleration of the vehicle body in dry sand. In an EV, the poles and zeros at the low-frequency side dominate in dry sand conditions. High-frequency vibration has little effect on the vertical acceleration of vehicle body. Thus, it is sufficient to apply the model to the low-frequency side of equation (12), which is expressed as equation (13).

$$G_{p1}(s)=\frac{M_{p1}}{s}\cdot\frac{(s^2+2\zeta_{z1}\omega_{z1}s+{\omega_{z1}}^2)}{(s^2+2\zeta_{p1}\omega_{p1}s+{\omega_{p1}}^2)} \tag{13}$$

$$M_{p1}=M_p\cdot\frac{{\omega_{z2}}^2}{{\omega_{p2}}^2}$$

The feedforward compensator, which consists of the reference model response $G_{r1}(s)$ and the inverse filter form of the transfer function $G_{p1}(s)$ of the plant, can be expressed as equation (15).

$$G_{rl}(s)=\frac{M_{p1}}{s}\cdot\frac{(s^2+2\zeta_{z1}\omega_{z1}s+{\omega_{z1}}^2)}{(s^2+2\omega_{p1}s+{\omega_{p1}}^2)} \tag{14}$$

$$\frac{G_{rl}(s)}{G_{pl}(s)}=\frac{(s^2+2\zeta_{p1}\omega_{p1}s+{\omega_{p1}}^2)}{(s^2+2\omega_{p1}s+{\omega_{p1}}^2)} \tag{15}$$

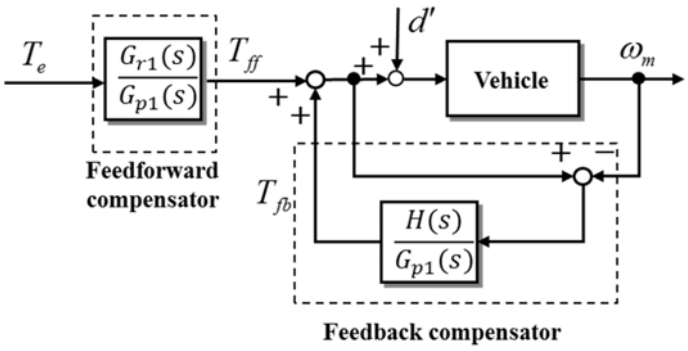

Figure 12: The proposed vibration control

Figure 12 shows that the notation H(s) is a band-pass filter; its central frequency coincides with the natural frequency of the vertical acceleration. The response of ω_m to the disturbance d can be derived by equation (17). When k = 1 in equation (16), the gain of (1 - H(s)) at the natural vibration frequency becomes zero. This indicates that the perfect zeroing of the natural vibration frequency was achieved.

$$H(s)=\frac{2k\omega_{p1}s}{(s^2+2\omega_{p1}s+{\omega_{p1}}^2)} \tag{16}$$

$$\omega_m = \big(1 - H(s)\big)G_{p1}(s)d \tag{17}$$

4.2 Effect of proposed vibration control strategy

The effect of the proposed vibration control strategy in Chapter 4.1 was evaluated using simulation and vehicle test. The simulation results are shown in Figure 13. Figure 13-a shows simulation results with vibration control off in the acceleration condition with a constant electric motor torque. Figure.13-b shows simulation results with vibration control on. Next, vehicle test results are shown in Figure 14. Figure 14-a shows vehicle test results with vibration control off. Figure 14-b shows vehicle test results with vibration control on.

Figure 13-a and Figure 14-a show the vertical acceleration of the vehicle body vibrate although the electric motor torque is constant. The speed change of the drive wheels by slip is the same as the vertical vibration frequency. Figure 14-a and Figure 14-b shows the new electric motor control strategy achieving smooth acceleration in dry sand conditions

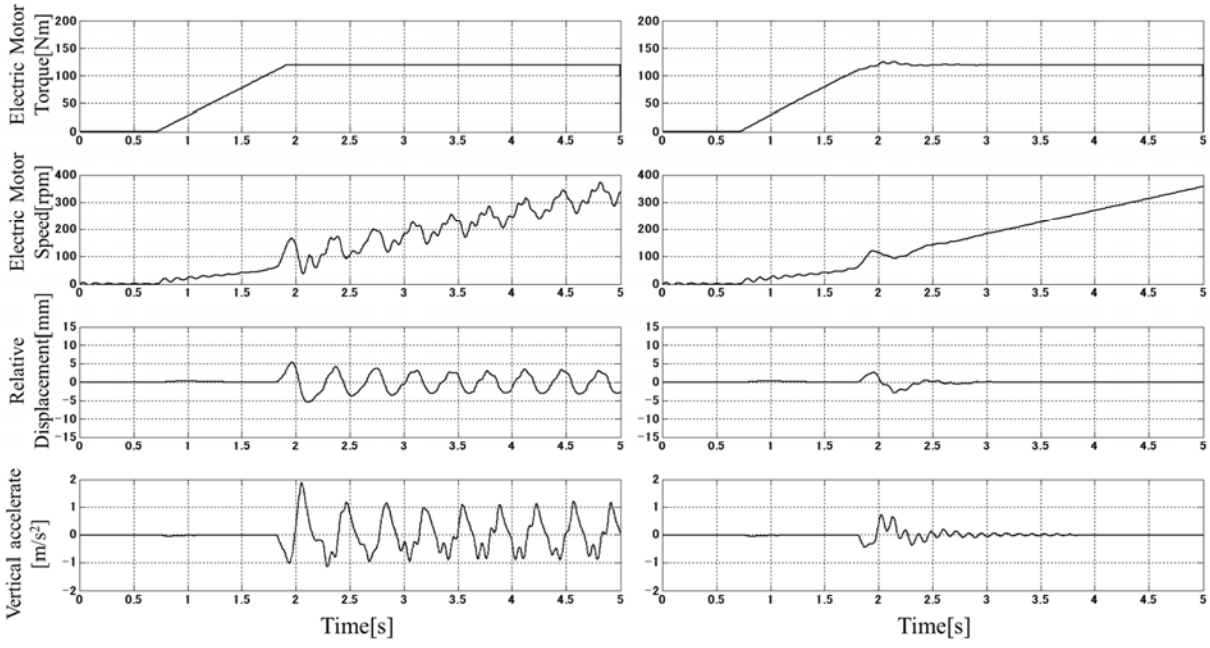

Figure 13-a: vibration control off

Figure 13-b: vibration control on

Figure 13: Simulation results

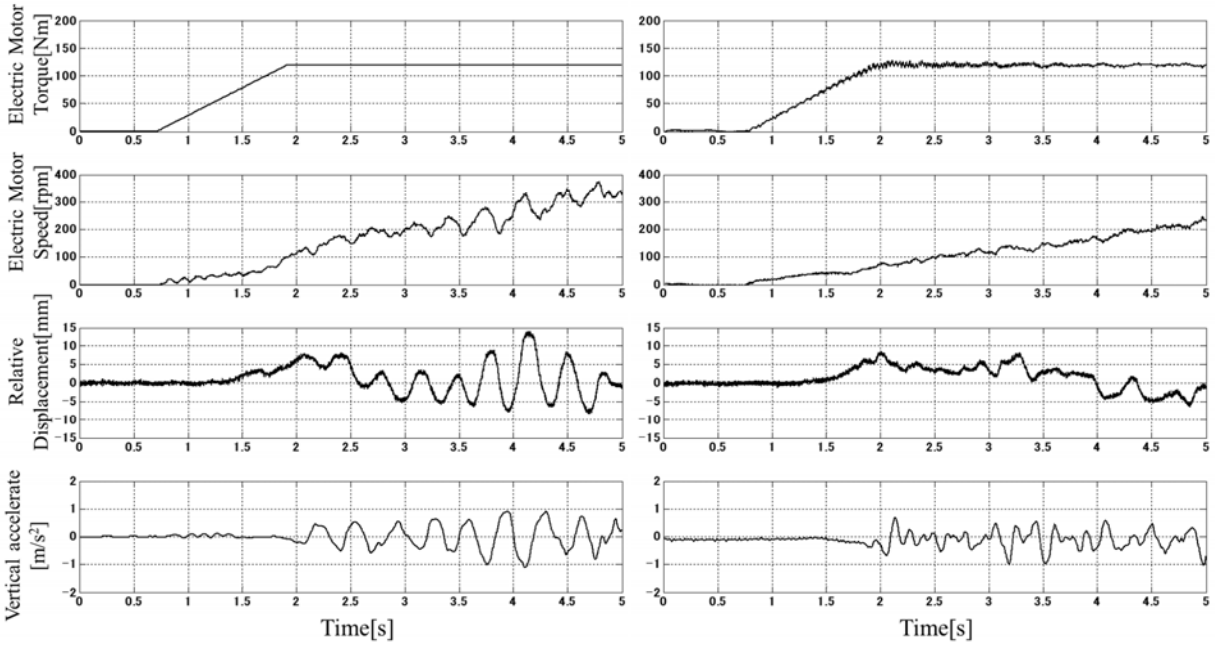

Figure 14-a: vibration control off

Figure 14-b: vibration control on

Figure 14: Experimental results

As a result, we applied a new electric motor control strategy to reduce motor speed fluctuations and vertical vibrations in dry sand conditions that suppress tire rotational speed caused by road disturbance. Figure 15 shows an estimated mechanism of vertical vibration in dry sand conditions. The vertical vibration of the tire and the vehicle body was reduced by suppressing the tire slip using vibration control in dry sand conditions.

i. Running on sand at the tire linear region.
ii. Increased tire sinkage and relative distance at the non-linear region.
iii. The slip speed decreases and the tire returns to the linear region after the body sinks.
iv. Decreased tire sinkage and relative distance at the tire linear region.
v. Maximum driving force decreased and the car body rises.

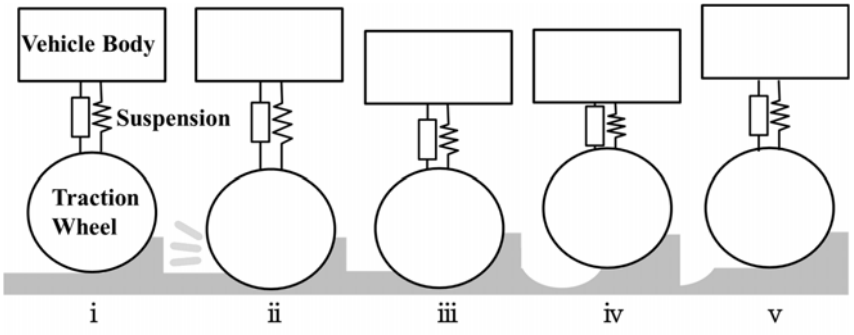

Figure 15: Estimated mechanism of vertical vibration

5 Conclusion

A simulation was conducted which considered the tire slip and the relative distance between the tire and the vehicle body to model and analyze the vertical vibration generated when an EV is driven in dry sand conditions. A motor control system was proposed, which enabled smooth running of the EV by suppressing the vertical vibration of the vehicle body.

References

[1] Hiromichi Kawamura, Ken Ito, Takaaki Karikomi, Tomohiro Kume, *Highly-Responsive Acceleration Control for the Nissan LEAF Electric Vehicle*, SAE Paper No.2011-01-0397 (2011)

[2] Ryosuke Eto, Junya Yamakawa*, Vehicle Motion Control Based on Tire Model on Dry Sand,* JSAE Congress (Autumn), 159 (2017)

[3] Wataru Kobayashi, Satoru Okubo*, the Development of Evaluation Method for AWD System by Constructing a Simulation Dynamo,* JSAE Congress (Autumn), 192 (2018)

[4] Akira Sawada, Katsunori Nakamura, Jun Motosugi, Kengo Fujiwara, Takashi Nakajima*, A Study on the Vertical Vibration of Electric Vehicle in Driving on Dry Sand,* JSAE Congress (Autumn), 60 (2020)

Presenter Biography

Akira Sawada graduated from Kinki University with a Bachelor of Science degree in Electromechanical Engineering in 2004.

2004-2020, Engineer of electric motor control, Nissan motor corporation.

2020-present, Assistant manager of electric motor control, developing the electric powertrain of new Nissan EV and e-POWER.